

**Figure 11** Average depth of magma lens reflections beneath ridges versus spreading rate. The curved line shows the depth to the 1200°C isotherm calculated from the ridge thermal model of Phipps Morgan J and Chen YJ (1993) *Journal of Geophysical Research* 98: 6283–6297. Data from different ridges are labeled Reykjanes Ridge (RR), Juan de Fuca Ridge (JdF), Costa Rica Rift (CRR), Lau Basin (Lau), northern and southern East Pacific Rise (NEPR and SEPR, respectively). (Reproduced from Carbotte SM, Mutter CZ, Mutter J and Ponce-Correa G (1998) *Geology* 26: 455–458.)

ition to deeper lenses at intermediate spreading rates, consistent with the present dataset (Figure 11).

However, there is no evidence for the systematic deepening of magma lenses within the intermediate to slow spreading range that is predicted by the numerical models (Figure 11). Instead, where magma lenses have been observed at these ridges, they cluster at 2.5–3 km depth. At these spreading

rates there may be large local variations in the supply of magma from the mantle to the axis that control ridge thermal structure and give rise to shallower magma lenses than predicted from spreading rate alone. In light of recent observations, the role of neutral buoyancy may need to be reconsidered. If the magma lens is not a region of 100% melt, magma densities may be considerably higher than used in previous neutral buoyancy calculations. The magma lens may indeed lie at its correct neutrality depth, and the observed variation in magma lens depth may reflect changes in the density of the melt and crystal aggregate found within the lens.

## See also

**Mid-ocean Ridge Geochemistry and Petrology. Mid-ocean Ridge Tectonics, Volcanism and Geomorphology. Seamounts and Off-ridge Volcanism. Seismic Structure.**

## Further Reading

- Buck WR, Delaney PT, Karson JA and Lagabrielle Y (eds) (1998) *Faulting and Magmatism at Mid-Ocean Ridges*, Geophysical Monograph 106. Washington, DC: American Geophysical Union.
- Detrick RS, Buhl P, Vera E *et al.* (1987) Multichannel seismic imaging of a crustal magma chamber along the East Pacific Rise. *Nature* 326: 35–41.
- Jacobson RS (1992) Impact of crustal evolution on changes of the seismic properties of the uppermost oceanic crust. *Reviews of Geophysics* 30: 23–42.
- Phipps Morgan J and Chen YJ (1993) The genesis of oceanic crust: magma injection, hydrothermal circulation, and crustal flow. *Journal of Geophysical Research* 98: 6283–6297.
- Sinton JA and Detrick RS (1991) Mid-ocean ridge magma chambers. *Journal of Geophysical Research* 97: 197–216.
- Solomon SC and Toomey DR (1992) The structure of mid-ocean ridges. *Annual Review of Earth and Planetary Sciences* 20: 329–364.

# MID-OCEAN RIDGE TECTONICS, VOLCANISM AND GEOMORPHOLOGY

**K. C. Macdonald**, Department of Geological Sciences and Marine Sciences Institute, University of California, Santa Barbara, CA, USA

Copyright © 2001 Academic Press

doi:10.1006/rwos.2001.0094

## Introduction

The midocean ridge is the largest mountain chain and the most active system of volcanoes in the solar system. In plate tectonic theory, the ridge is located between plates of the earth's rigid outer shell that

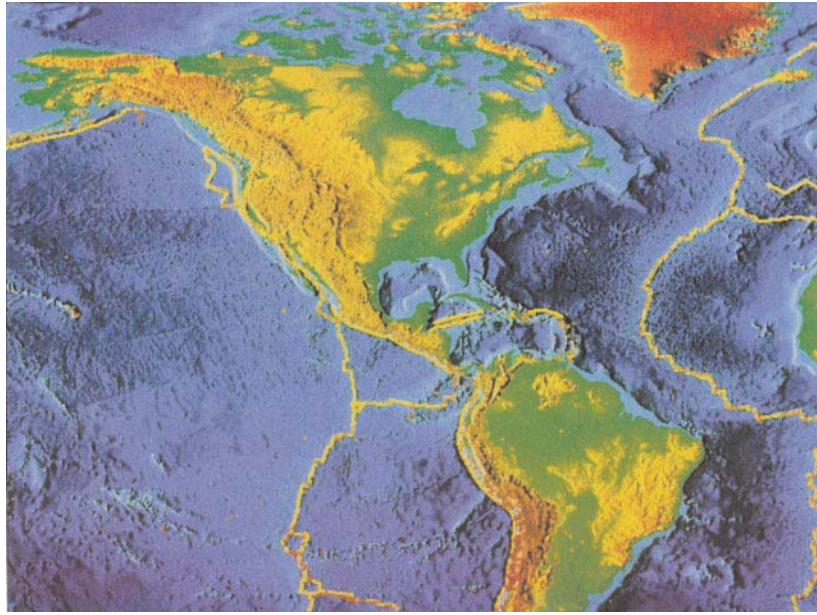


**Figure 1** Shaded relief map of the seafloor showing parts of the East Pacific Rise, a fast-spreading center, and the Mid-Atlantic Ridge, a slow-spreading center. Courtesy of National Geophysical Data Center.

are separating at speeds of  $\sim 10$  to  $170 \text{ mm y}^{-1}$  (up to  $220 \text{ mm y}^{-1}$  in the past). The ascent of molten rock from deep in the earth ( $\sim 30\text{--}60 \text{ km}$ ) to fill the void between the plates creates new seafloor and a volcanically active ridge. This ridge system wraps around the globe like the seam of a baseball and is approximately  $70\,000 \text{ km}$  long. Yet the ridge itself is only  $\sim 5\text{--}30 \text{ km}$  wide – very small compared to the plates, which can be thousands of kilometers across (Figure 1).

Early exploration showed that the gross morphology of spreading centers varies with the rate of plate separation. At slow spreading rates ( $10\text{--}40 \text{ mm y}^{-1}$ ) a  $1\text{--}3 \text{ km}$  deep rift valley marks the axis, while for fast spreading rates ( $> 90 \text{ mm y}^{-1}$ ) the axis is characterized by an elevation of the seafloor of several hundred meters, called an axial high (Figure 2). The rate of magma supply is a second factor that may influence the morphology of midocean ridges. For example, a very high rate of magma supply can produce an axial high even where the spreading rate is slow; the Reykjanes Ridge south of Iceland is a good example. Also, for intermediate spreading rates ( $40\text{--}90 \text{ mm y}^{-1}$ ) the ridge crest may have either an axial high or rift valley depending on the rate of magma supply. The seafloor deepens from a global average of  $\sim 2600 \text{ m}$  at the spreading center to  $> 5000 \text{ m}$  beyond the ridge flanks. The rate of deepening is proportional to the square root of the age of the seafloor because

it is caused by the thermal contraction of the lithosphere. Early mapping efforts also showed that the midocean ridge is a discontinuous structure that is offset at right angles to its length at numerous transform faults tens to hundreds of kilometers in length.

Maps are powerful; they inform, excite, and stimulate. Just as the earliest maps of the world in the sixteenth century ushered in a vigorous age of exploration, the first high-resolution, continuous coverage maps of the midocean ridge stimulated investigators from a wide range of fields including petrologists, geochemists, volcanologists, seismologists, tectonicists, and practitioners of marine magnetism and gravity; as well as researchers outside the earth sciences including marine ecologists, chemists, and biochemists. Marine geologists have found that many of the most revealing variations are to be observed by exploring along the axis of the active ridge. This along-strike perspective has revealed the architecture of the global rift system. The ridge axis undulates up and down in a systematic way, defining a fundamental partitioning of the ridge into segments bounded by a variety of discontinuities. These segments behave like giant cracks in the seafloor that can lengthen or shorten, and have episodes of increased volcanic and tectonic activity.

Another important change in perspective came from the discovery of hydrothermal vents by marine geologists and geophysicists. It became clear that in

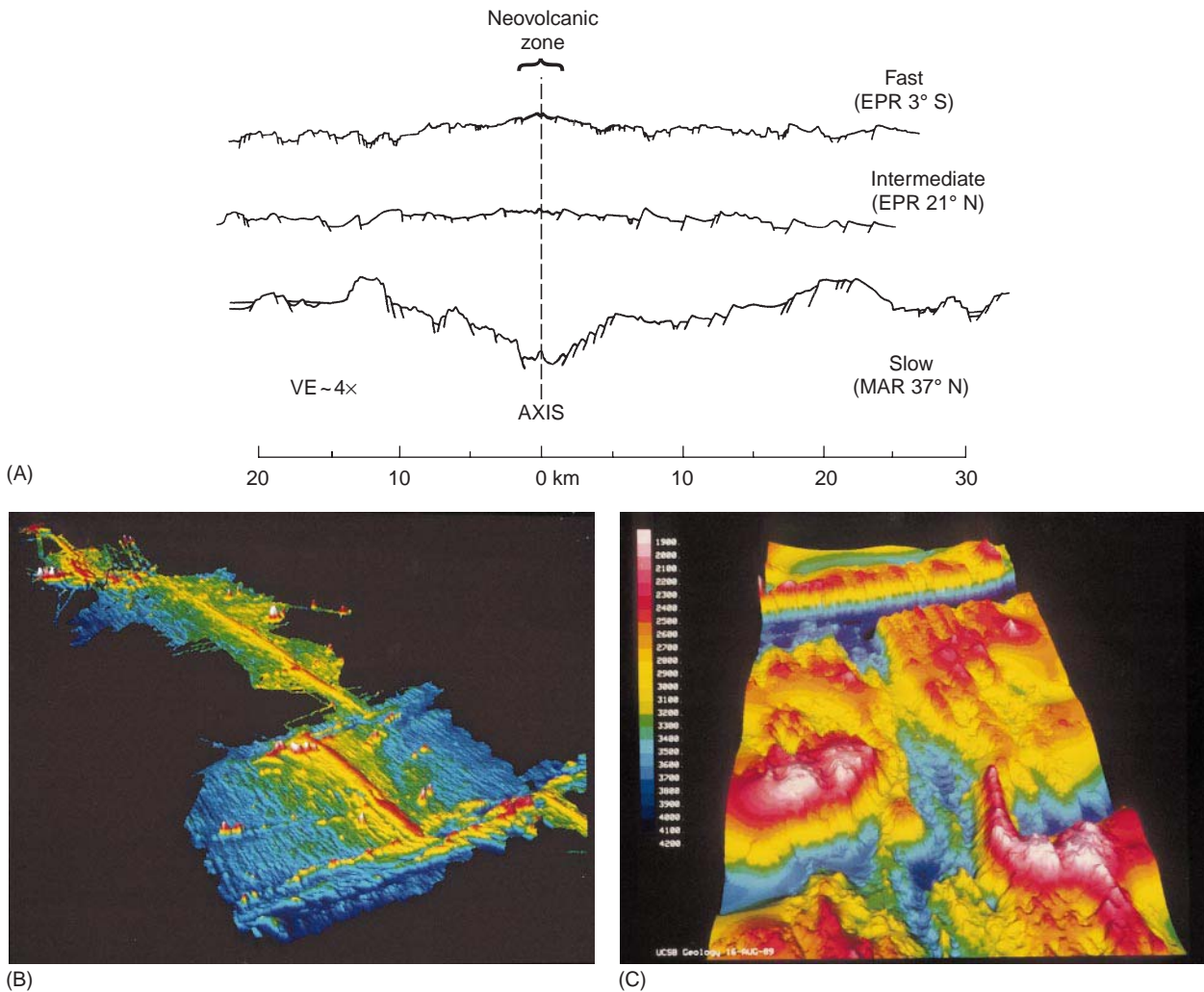


**Figure 2** Topography of spreading centers. (A) Cross-sections of typical fast-, intermediate-, and slow-spreading ridges based on high resolution deep-tow profiles. The neovolcanic zone is noted (the zone of active volcanism) and is several kilometers wide; the zone of active faulting extends to the edge of the profiles and is several tens of kilometers wide. After Macdonald *et al.* (1982). (B) Shaded relief map of a 1000km stretch of the East Pacific Rise extending from 8° to 17°N. Here, the East Pacific Rise is the boundary between the Pacific and Cocos plates, which separate at a 'fast' rate of  $110\text{mm y}^{-1}$ . The map reveals two kinds of discontinuities: large offsets, about 100 km long, known as transform faults and smaller offsets, about 10 km long, called overlapping spreading centers. Colors indicate depths of from 2400 m (pink) to 3500 m (dark blue). (C.) Shaded relief map of the Mid-Atlantic Ridge. Here, the ridge is the plate boundary between the South American and African plates, which are spreading apart at the slow rate of approximately  $35\text{mm y}^{-1}$ . The axis of the ridge is marked by a 1–2 km deep rift valley, which is typical of most slow-spreading ridges. The map reveals a 12 km jog of the rift valley, a second-order discontinuity, and also shows a first-order discontinuity called the Cox transform fault. Colors indicated depths of from 1900 m (pink) to 4200 m (dark blue).

studies of midocean ridge tectonics, volcanism, and hydrothermal activity, the greatest excitement is in the linkages between these different fields. For example, geophysicists searched for hydrothermal activity on mid-ocean ridges for many years by towing arrays of thermistors near the seafloor. However, hydrothermal activity was eventually documented more effectively by photographing the distribution of exotic vent animals. Even now, the best indi-

cators of the recency of volcanic eruptions and the duration of hydrothermal activity emerge from studying the characteristics of benthic faunal communities. For example, during the first deep-sea midocean ridge eruption witnessed from a submersible, divers did not see a slow lumbering cascade of pillow lavas as observed by divers off the coast of Hawaii. What they saw was completely unexpected: white bacterial matting billowing out of the sea-

floor, creating a scene much like a midwinter blizzard in Iceland, covering all of the freshly erupted, glassy, black lava with a thick blanket of white bacterial 'snow'.

### Large-scale Variations in Axial Morphology; Correlations with Magma Supply and Segmentation

The axial depth profile of midocean ridges undulates up and down with a wavelength of tens of kilometers and amplitude of tens to hundreds of meters at fast and intermediate rate ridges. This same pattern is observed for slow-spreading ridges as well, but the wavelength of undulation is shorter and the amplitude is larger (Figure 3). In most cases, ridge axis discontinuities (RADs) occur at local maxima along the axial depth profile. These discontinuities include transform faults (first order); overlapping spreading centers (OSCs, second order) and higher-order (third-, fourth-order) discontinuities, which are increasingly short-lived, mobile, and associated with smaller offsets of the ridge (see Table 1 and Figure 4).

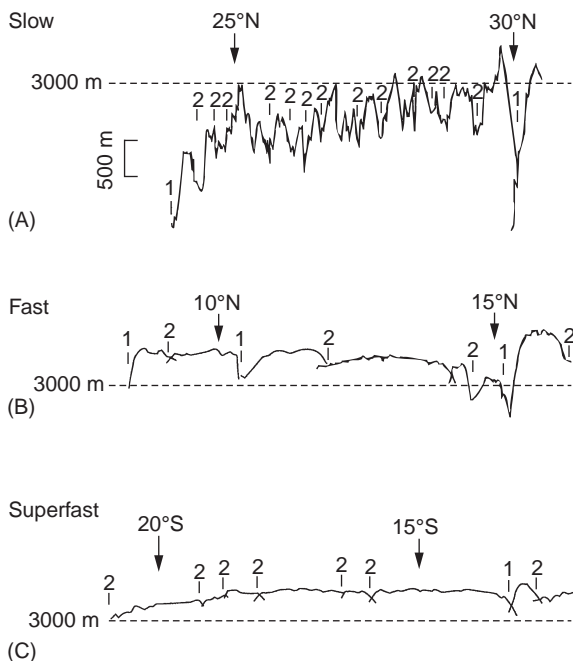


**Figure 3** Axial depth profiles for (A) slow-spreading and (B) fast-spreading, and (C) ultrafast-spreading ridges. Discontinuities of orders 1 and 2 typically occur at local depth maxima (discontinuities of orders 3 and 4 are not labeled here). The segments at faster spreading rates are longer and have smoother, lower-amplitude axial depth profiles. These depth variations may reflect the pattern of magma delivery to the ridge.

A much-debated hypothesis is that the axial depth profile (Figures 3 and 5) reflects the magma supply along a ridge segment. According to this idea, the magma supply is enhanced along shallow portions of ridge segments and is relatively starved at segment ends (at discontinuities). In support of this hypothesis is the observation at ridges with an axial high (fast-spreading ridges) that the cross-sectional area or axial volume varies directly with depth (Figure 6). Maxima in cross-sectional area ( $> 2.5 \text{ km}^2$ ) occur at minima along the axial depth profile (generally not near RADs) and are thought to correlate with regions where magma supply is robust. Conversely, small cross-sectional areas ( $< 1.5 \text{ km}^2$ ) occur at local depth maxima and are interpreted to reflect minima in the magma supply rate along a given ridge segment. On slow-spreading ridges characterized by an axial rift valley, the cross-sectional area of the valley is at a minimum in the mid-segment regions where the depth is minimum. In addition, there are more volcanoes in the shallow midsegment area, and fewer volcanoes near the segment ends. Studies of crustal magnetization show that very highly magnetized zones occur near segment ends, which is most easily explained by a locally starved magma supply resulting in the eruption of highly fractionated lavas rich in iron.

Multichannel seismic and gravity data support the axial volume/magma supply/segmentation hypothesis (Figure 6). A bright reflector, which is phase-reversed in many places, occurs commonly ( $> 60\%$  of ridge length) beneath the axial region of both the northern and southern portions of the fast- and ultra-fast spreading East Pacific Rise (EPR). This reflector has been interpreted to be a thin lens of magma residing at the top of a broader axial magma reservoir. The amount of melt is highly variable along-strike varying from a lens that is primarily crystal mush to one that is close to 100% melt. This 'axial magma chamber' (AMC) reflector is observed where the ridge is shallow and where the axial high has a broad cross-sectional area. Conversely, it is rare where the ridge is deep and narrow, especially near RADs. A reflector may occur beneath RADs during events of propagation and ridge-axis realignment, as may be occurring now on the EPR near  $9^\circ\text{N}$ .

There is evidence that major-element geochemistry correlates with axial-cross-sectional area (Figure 7). On the EPR  $13^\circ\text{--}21^\circ\text{S}$ , there is a good correlation between MgO wt% and cross-sectional area (high MgO indicates a higher eruption temperature and perhaps a greater local magmatic budget). The abundance of hydrothermal venting (as measured by

**Table 1** Characteristics of segmentation. This four-tiered hierarchy of segmentation probably represents a continuum in segmentation

	Order 1	Order 2	Order 3	Order 4
<i>Segments</i>				
Segment length (km)	600 ± 300 <sup>a</sup> (400 ± 200) <sup>b</sup>	140 ± 90 (50 ± 30)	20 ± 10 (15 ± 10?)	7 ± 5 (7 ± 5?)
Segment longevity (years)	> 5 × 10 <sup>6</sup>	0.5–5 × 10 <sup>6</sup> (0.5–30 × 10 <sup>6</sup> )	~ 10 <sup>4</sup> –10 <sup>5</sup> (?)	< 10 <sup>3</sup> (?)
Rate of segment lengthening (long term migration) mm y <sup>-1</sup>	0–50 (0–30)	0–1000 (0–30)	Indeterminate: no off-axis trace	Indeterminate: no off-axis trace
Rate of segment lengthening (short term propagation) mm y <sup>-1</sup>	0–100 (?)	0–1000 (0–50)	Indeterminate: no off-axis trace	Indeterminate: no off-axis trace
<i>Discontinuities</i>				
Type	Transform, large propagating rifts	Overlapping spreading centers (oblique shear zones, rift valley jogs)	Overlapping spreading centers (intervolcano gaps), devails	Devails, offsets of axial summit caldera (intravolcano gaps)
Offset (km)	> 30	2–30	0.5–2.0	< 1
Offset age (years) <sup>c</sup>	> 0.5 × 10 <sup>6</sup> ( > 2 × 10 <sup>6</sup> )	0.5 × 10 <sup>6</sup> (2 × 10 <sup>6</sup> )	~ 0	~ 0
Depth anomaly	300–600 (500–2000)	100–300 (300–1000)	30–100 (50–300)	0–50 (0–100?)
Off-axis trace	Fracture zone	V-shaped discordant zone	Faint or none	None
High amplitude magnetization?	Yes	Yes	Rarely (?)	No? (?)
Breaks in axial magma chamber?	Always	Yes, except during OSC linkage? (NA)	Yes, except during OSC linkage? (NA)	Rarely
Breaks in axial low-velocity zone?	Yes (NA)	No, but reduction in volume (NA)	Small reduction in volume (NA)	Small reduction in volume? (NA)
Geochemical anomaly?	Yes	Yes	Usually	~ 50%
Break in high-temperature venting?	Yes	Yes	Yes (NA)	Often (NA)

<sup>a</sup>Values are ± 1 standard deviation.

<sup>b</sup>Where information differs for slow- versus fast-spreading ridges (< 60 mm y<sup>-1</sup>), it is placed in parentheses.

<sup>c</sup>Offset age refers to the age of the seafloor that is juxtaposed to the spreading axis at a discontinuity.

Updated from Macdonald *et al.* (1991).

NA, not applicable; ?, not presently known as poorly constrained.

light transmission and backscatter in the water column and geochemical tracers) also varies directly with the cross-sectional area of the EPR. It is not often that one sees a correlation between two such different kinds of measurements. It is all the more remarkable considering that the measurements of hydrothermal activity are sensitive to changes on a timescale of days to months, while the cross-sectional area probably reflects a timescale of change measured in tens of thousands of years.

On slow-spreading centers, such as the Mid-Atlantic Ridge (MAR), the picture is less clear. Seismic and gravity data indicate that the oceanic crust thins significantly near many transform faults,

even those with a small offset. This is thought to be the result of highly focused mantle upwelling near mid-segment regions, with very little along axis flow of magma away from the upwelling region. Focused upwelling is inferred from ‘bulls-eye’-shaped residual gravity anomalies and by crustal thickness variations documented by seismic refraction and microearthquake studies. At slow-spreading centers, melt probably resides in small, isolated, and very short-lived pockets beneath the median valley floor (Figure 5C) and beneath elongated axial volcanic ridges. An alternative view is that the observed along-strike variations in topography and crustal thickness can be accounted for by along-strike vari-

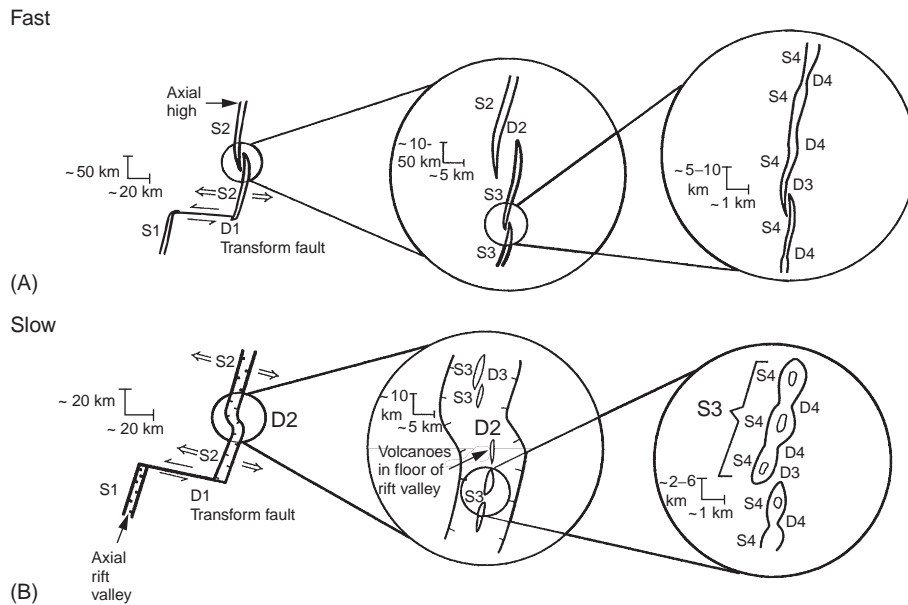


**Figure 4** A possible hierarchy of ridge segmentation for (A) fast-spreading and (B) slow-spreading ridges. S1–S4 are ridge segments or order 1–4, and D1–D4 are ridge axis discontinuities of order 1–4. At both fast- and slow-spreading centers, first-order discontinuities are transform faults. Examples of second-order discontinuities are overlapping spreading centers (OSCs) on fast-spreading ridges and oblique shear zones on slow-spreading ridges. Third-order discontinuities are small OSCs on fast-spreading ridges. Fourth-order discontinuities are slight bends or lateral offsets of the axis of less than 1 km on fast-spreading ridges. This four-tiered hierarchy of segmentation is probably a continuum; it has been established, for example, that fourth-order segments and discontinuities can grow to become third-, second-, and even first-order features and vice versa at both slow- and fast-spreading centers. Updated from Macdonald *et al.* (1991).

ations in mechanical thinning of the crust by faulting. There is no conflict between these models, so both focused upwelling and mechanical thinning may occur along each segment.

One might expect the same to hold at fast-spreading centers, i.e., crustal thinning adjacent to OSCs. This does not appear to be the case at 9°N on the EPR, where seismic data suggest a thickening of the crust toward the OSC and a widening of the AMC reflector. There is no indication of crustal thinning near the Clipperton transform fault either. And yet, as one approaches the 9°N OSC from the north, the axial depth plunges, the axial cross-sectional area decreases, the AMC reflector deepens, average lava age increases, MgO in dredged basalts decreases; hydrothermal activity decreases dramatically, crustal magnetization increases significantly (suggesting eruption of more fractionated basalts in a region of decreased magma supply), crustal fracturing and inferred depth of fracturing increases (indicating a greater ratio of extensional strain to magma supply), and the throw of off-axis normal faults increases (suggesting thicker lithosphere and greater strain) (Figure 8). How can these parameters all correlate so well, indicating a decrease in the magmatic budget and an increase in amagmatic

extension, while the seismic data suggest crustal thickening off-axis from the OSC and a wider magma lens near the OSC?

One possibility is that mantle upwelling and the axial magmatic budget are enhanced away from RADs even at fast-spreading centers, but that subaxial flow of magma ‘downhill’ away from the injection region redistributes magma (Figure 5). This along-strike flow and redistribution of magma may be unique to spreading centers with an axial high such as the EPR or Reykjanes where the axial region is sufficiently hot at shallow depths to facilitate subaxial flow. It is well documented in Iceland and other volcanic areas analogous to midocean ridges that magma can flow in subsurface chambers and dikes for distances of many tens of kilometers away from the source region before erupting. In this way, thicker crust may occur away from the midsegment injection points, proximal to discontinuities such as OSCs.

Based on studies of the fast-spreading EPR, a ‘magma supply’ model has been proposed that explains the intriguing correlation between over a dozen structural, geochemical and geophysical variables within a first-, second-, or third-order segment (Figure 9). It also addresses the initially

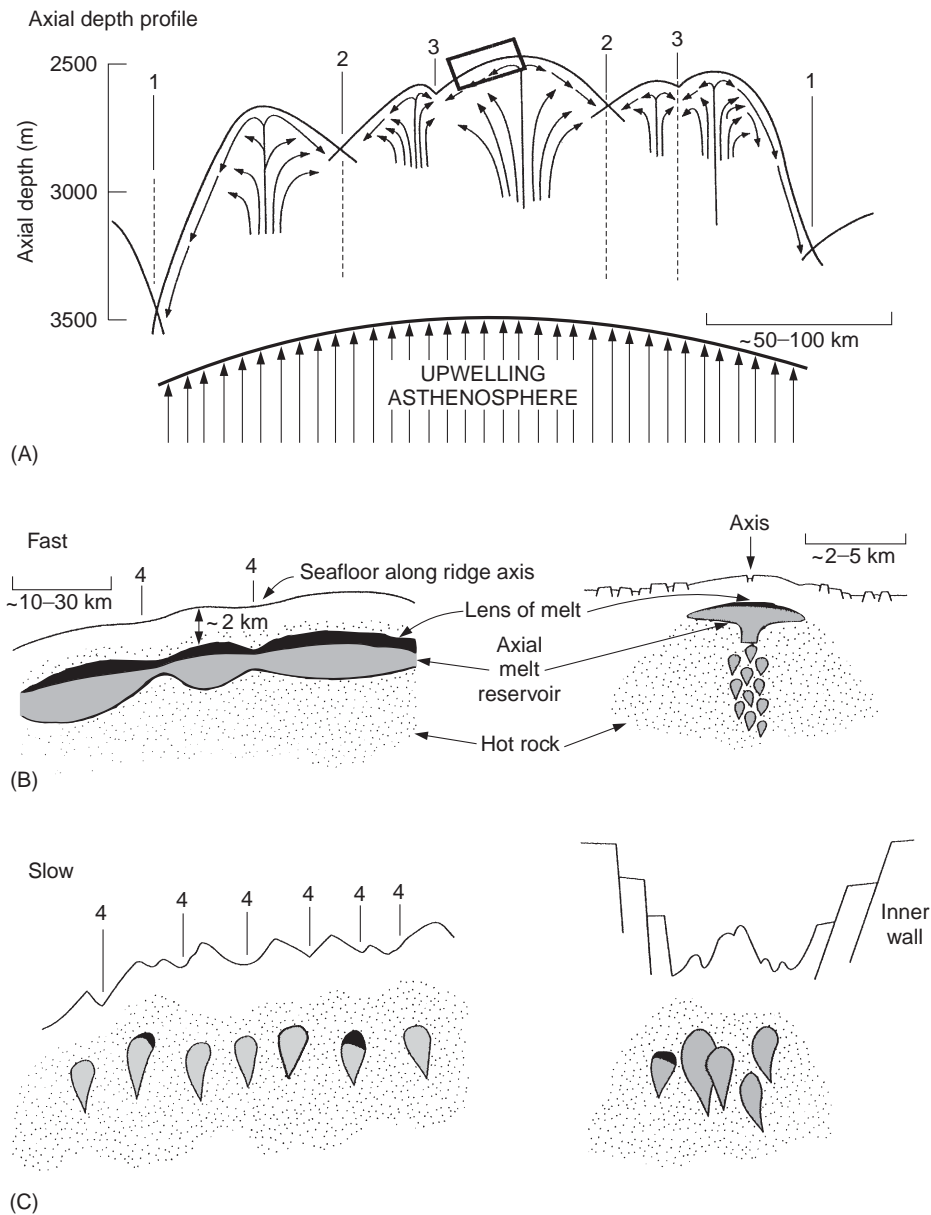


**Figure 5** Schematic diagram of how ridge segmentation may be related to mantle upwelling (A), and the distribution of magma supply (B and C). In (A), the depth scale applies only to the axial depth profile; numbers denote discontinuities and segments of orders 1–3. Decompression partial melting in upwelling asthenosphere occurs at depths 30–60 km beneath the ridge. As the melt ascends through a more slowly rising solid residuum, it is partitioned at different levels to feed segments of orders 1–3. Mantle upwelling is hypothesized to be ‘sheetlike’ in the sense that melt is upwelling along the entire length of the ridge; but the supply of melt is thought to be enhanced beneath shallow parts of the ridge away from major discontinuities. The rectangle is an enlargement to show fine-scale segmentation for (B) a fast-spreading example, and (C) a slow-spreading example. In (B) and (C) along-strike cross-sections showing hypothesized partitioning of the magma supply relative to fourth-order discontinuities (4s) and segments are shown on the left. Across-strike cross-sections for fast- and slow-spreading ridges are shown on the right. Updated from Macdonald *et al.* (1991).

puzzling observation that crust is sometimes thinner in the midsegment region where upwelling is supposedly enhanced. Intuitively, one might expect crust to be thickest over the region where upwelling is enhanced as observed on the MAR. However, along-axis redistribution of melt may be the control-

ling factor on fast-spreading ridges where the sub-axial melt region may be well-connected for tens of kilometers. In this model, temporal variations in along-axis melt connectivity may result in thicker crust near mid-segment when connectivity is low (most often slow-spreading ridges), and thicker crust

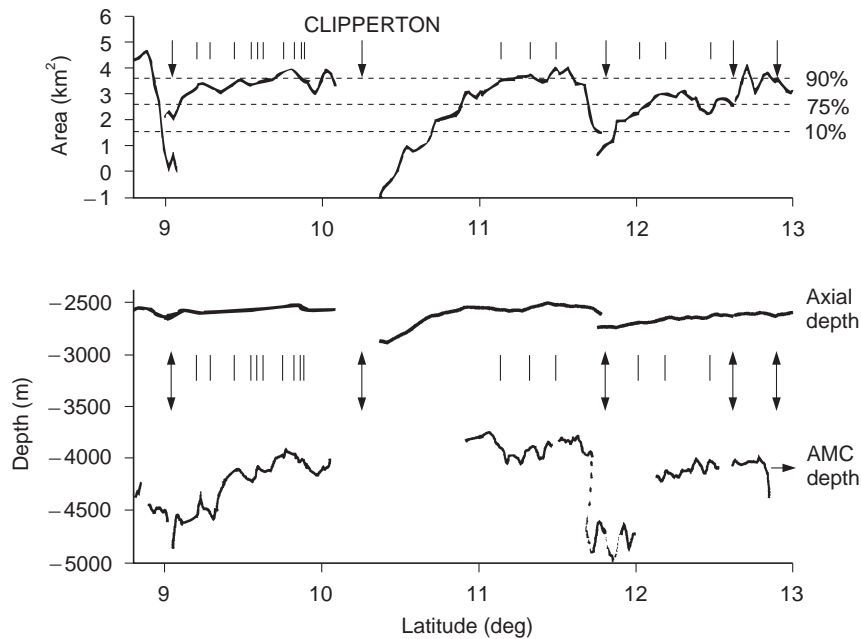


**Figure 6** Profiles of the along-axis cross-sectional area, depth, and axial magma chamber (AMC) seismic reflector for the EPR 9°–13°N. The locations of first- and second-order discontinuities are denoted by vertical arrows (first-order discontinuities are named); each occurs at a local minimum of the ridge area profile, and a local maximum in ridge axis depth. Lesser discontinuities are denoted by vertical bars. There is an excellent correlation between ridge axis depth and cross-sectional area; there is a good correlation between cross-sectional area and the existence of an axial magma chamber, but detailed characteristics of the axial magma chamber (depth, width) do not correlate. Updated from Scheirer and Macdonald (1993) and references therein.

closer to the segment ends when connectivity is high (most often, but not always the case at fast-spreading ridges).

The basic concepts of this magma supply model also apply to slow-spreading ridges characterized by an axial rift valley. Mantle melting is enhanced beneath the midsegment regions. However, the axial region is colder (averaged over time) and along-strike redistribution of melt is impeded. Thus, the crust tends to be thickest near the midsegment regions and thinnest near RADs (Figures 8 and 9).

### Fine-scale Variations in Ridge Morphology within the Axial Neovolcanic Zone

The axial neovolcanic zone occurs on or near the axis of the axial high on fast-spreading centers, or within the floor of the rift valley on slow-spreading centers (Figure 5B and C, right). Studies of the widths of the polarity transitions of magnetic anomalies, including *in situ* measurements from the research submersible *Alvin*, document that ~90% of the volcanism that creates the extrusive layer of oceanic crust occurs in a region 1–10 km wide at most spreading centers. Direct qualitative estimates of lava age at spreading centers using

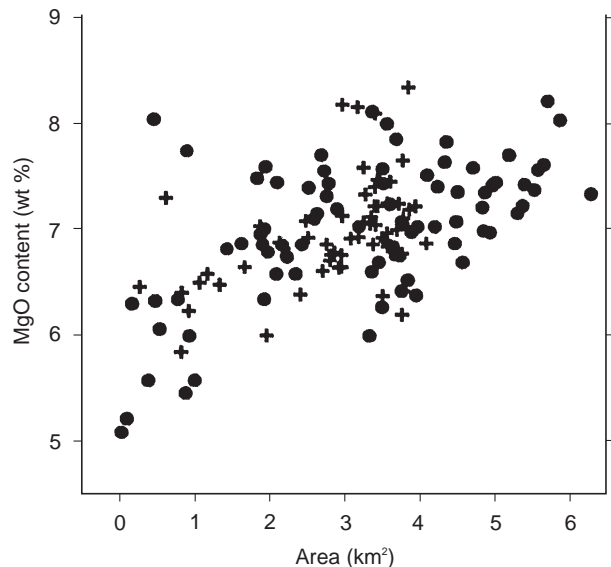


**Figure 7** Cross-sectional area of the East Pacific Rise versus MgO content of basalt glass (crosses from EPR 5–14°N, solid circles from 13–23°S). There is a tendency for high MgO contents (interpreted as higher eruption temperatures and perhaps higher magmatic budget) to correlate with larger cross-sectional area. Smaller cross-sectional areas correlate with lower MgO and a greater scatter in MgO content, suggesting magma chambers which are transient and changing. Thus shallow, inflated areas of the ridge tend to erupt hotter lavas. Updated from Scheirer and Macdonald (1993) and references therein.

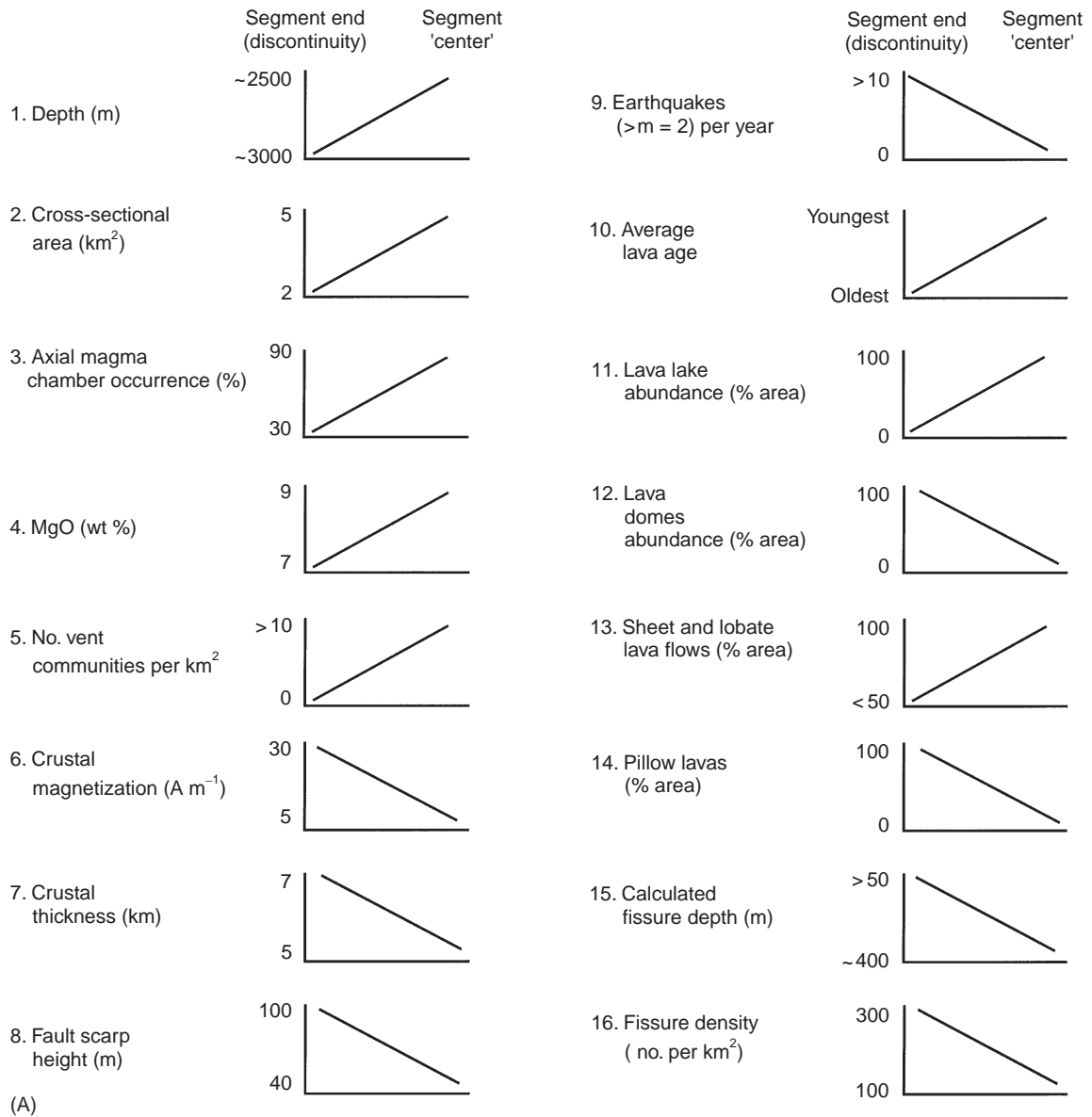


**Figure 8** Schematic summary of along-axis variations in spreading center properties from segment end (discontinuity of order 1, 2, or 3) to segment mid-section areas for (A) fast-spreading ridges with axial highs and (B) slow-spreading ridges with axial rift valleys. A large number of parameters correlate well with location within a given segment, indicating that segments are distinct, independent units of crustal accretion and deformation. These variations may reflect a fundamental segmentation of the supply of melt beneath the ridge. (Less than 1% of the ridge has been studied in sufficient detail to create this summary.)

submersibles and remotely operated vehicles (ROVs) tend to confirm this, as well as recent high-resolution seismic measurements that show that layer 2A (interpreted to be the volcanic layer) achieves its full thickness within 1–5 km of the rise axis. However, there are significant exceptions, including small volume off-axis volcanic constructions and voluminous off-axis floods of basaltic sheet flows.

The axial high on fast- and intermediate-spreading centers is usually bisected by an axial summit trough ~10–200 m deep that is found along approximately 60–70% of the axis. Along the axial high of fast-spreading ridges, sidescan sonar records show that there is an excellent correlation between the presence of an axial summit trough and an AMC reflector as seen on multichannel seismic records (>90% of ridge length). Neither axial

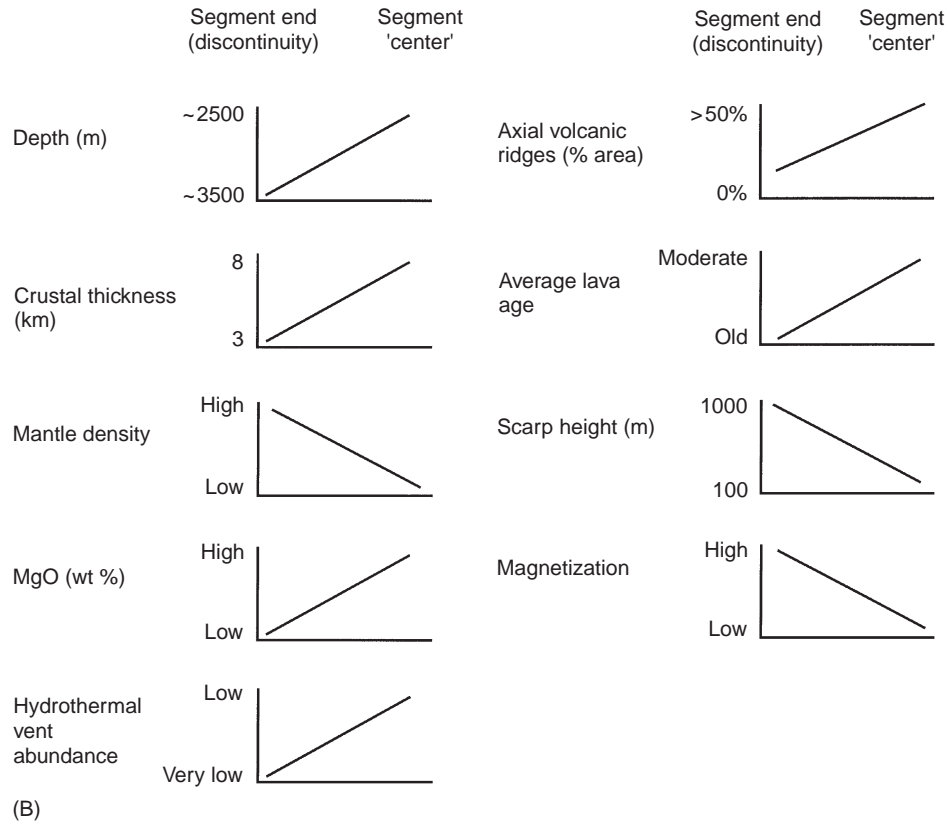


Figure 8 Continued

summit troughs nor AMCs occur where the ridge has a very small cross-sectional area.

In rare cases, an axial summit trough is not observed where the cross-sectional area is large. In these locations, volcanic activity is occurring at present or has been within the last decade. For example, on the EPR near 9°45'–52'N, a volcanic eruption documented from the submersible ALVIN was associated with a single major dike intrusion, similar to the 1993 eruption on the Juan de Fuca Ridge. Sidescan sonar records showed that an axial trough was missing from 9°52'N to 10°02'N, and in subsequent dives it was found that dike intrusion had propagated into this area, producing very recent lava flows and hydrothermal activity complete with bacterial 'snow-storms.' A similar situation has been thoroughly documented at 17°25'–30'S on the EPR where the axial cross-sectional area is large but the axial summit trough is partly filled. Perhaps the axial summit trough has been flooded with lava so recently that magma withdrawal and summit collapse is just occurring now. Thus, the presence of an axial summit trough along the axial high of a fast-spreading ridge is a good indicator of the presence of a subaxial lens of partial melt (AMC); where an

axial summit trough is not present but the cross-sectional area is large, this is a good indicator of very recent or current volcanic eruptions; where an axial summit trough is not present and the cross-sectional area is small, this is a good indicator of the absence of a magma lens (AMC).

In contrast to the along-axis continuity of the axial neovolcanic zone on fast-spreading ridges, the neovolcanic zone on slower-spreading ridges is considerably less continuous and there is a great deal of variation from segment to segment. Volcanic constructions, called axial volcanic ridges, are most common along the shallow, mid-segment regions of the axial rift valley. Near the ends of segments where the rift valley deepens, widens, and is truncated by transform faults or oblique shear zones, the gaps between axial volcanic ridges become longer. The gaps between axial volcanic ridges are regions of older crust characterized by faulting and a lack of recent volcanism. These gaps may correspond to fine-scale (third- and fourth-order) discontinuities of the ridge.

Another important difference between volcanism on fast- and slow-spreading ridges is that axial volcanic ridges represent a thickening of the volcanic

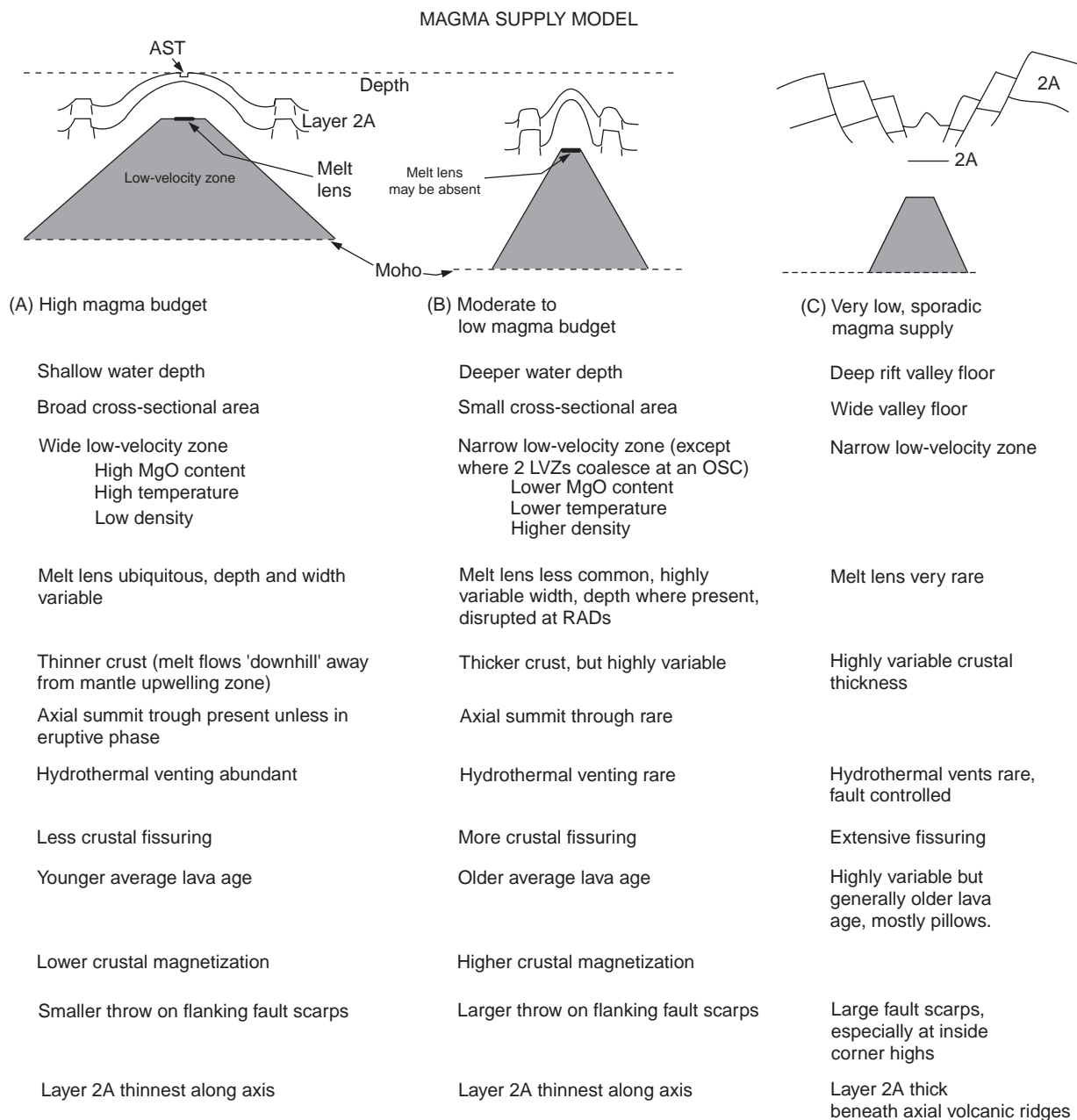


**Figure 9** Magma supply model for mid-ocean ridges (see references in Buck *et al.*, 1998). (A) represents a segment with a robust magmatic budget, generally a fast-spreading ridge away from discontinuities or a hotspot dominated ridge with an axial high (AST is the axial summit trough). (B) represents a segment with a moderate magma budget, generally a fast-spreading ridge near a discontinuity or a nonrifted intermediate rate ridge. (C) represents a ridge with a sporadic and diminished magma supply, generally a rifted intermediate to slow rate spreading center (for along-strike variations at a slow ridge, see Fig. 8B).

layer atop a lithosphere that may be 5–10 km thick, even on the axis. In contrast, the volcanic layer is usually thinnest along the axis of the EPR. Thus the axial high on fast-spreading ridges is not a thickened accumulation of lava, while the discontinuous axial volcanic ridges on slow-spreading ridges are.

On both slow- and fast-spreading ridges, pillow and lobate lavas are the most common lava morphology. Based on laboratory studies and observations of terrestrial basaltic eruptions, this means that the lava effusion rates are slow to moderate on most midocean ridges. High volcanic effusion rates, indicated by fossil lava lakes and extensive outcrops

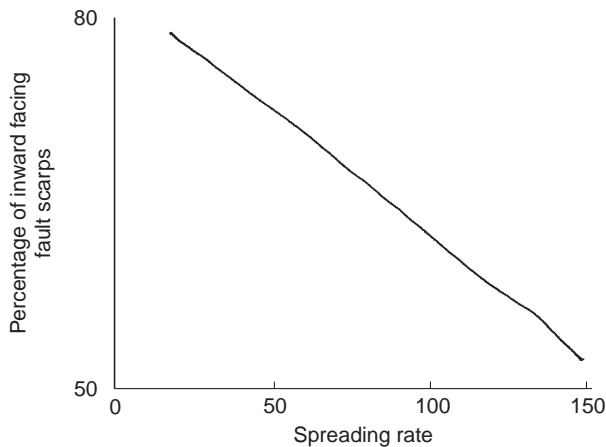


**Figure 10** Spreading rate versus percentage of fault scarps that are inward-facing (facing toward the spreading axis versus away from the spreading axis). A significant increase in the percentage of inward-facing scarps occurs at slower spreading rates.

of sheet flow lava morphology, are very rare on slow-spreading ridges. High effusion rate eruptions are more common on fast-spreading ridges and are more likely to occur along the shallow, inflated midsegment regions of the rise, in keeping with the magma supply model for ridges discussed earlier. Low effusion rate flows, such as pillow lavas, dominate at segment ends (Figure 8A).

Very little is known about eruption frequency. It has been estimated based on some indirect observations that at any given place on a fast-spreading ridge eruptions occur approximately every 5–100 years, and that on slow-spreading ridges it is approximately every 5000–10 000 years. If this is true, then the eruption frequency varies inversely with the spreading rate squared. On intermediate- to fast-spreading centers, if one assumes a typical dike width of  $\sim 50$  cm and a spreading rate of  $5\text{--}10\text{ cm y}^{-1}$ , then an eruption could occur  $\sim$  every 5–10 years. This estimate is in reasonable agreement with the occurrence of megaplumes and eruptions on the well-monitored Juan de Fuca Ridge. However, observations in sheeted dike sequences in Iceland and ophiolites indicate that only a small percentage of the dikes reach the surface to produce eruptions.

On fast-spreading centers, the axial summit trough is so narrow (30–1000 m) and well-defined in most places that tiny offsets and discontinuities of the rise axis can be detected (Table 1, Figure 2). This finest scale of segmentation (fourth-order segments and discontinuities) probably corresponds to individual fissure eruption events similar to the Krafla eruptions in Iceland or the Kilauea east rift

zone eruptions in Hawaii. Given a magma chamber depth of 1–2 km, an average dike ascent rate of  $\sim 0.1\text{ km h}^{-1}$  and an average lengthening rate of  $\sim 1\text{ km h}^{-1}$ , typical diking events would give rise to segments 10–20 km long. This agrees with observations of fourth-order segmentation and the scale of the recent diking event on the Juan de Fuca Ridge and in other volcanic rift zones. The duration of such segments is thought to be very short,  $\sim 100\text{--}1000$  years (too brief in any case to leave even the smallest detectable trace off-axis, Table 1). Yet even at this very fine scale, excellent correlations can be seen between average lava age, density of fissuring, the average widths of fissures, and abundance of hydrothermal vents within individual segments. In fact there is even an excellent correlation between ridge cross-sectional area and the abundance of benthic hydrothermal communities (Figure 8).

A curious observation on the EPR is that the widest fissures occur in the youngest lava fields. If fissures grow in width with time and increasing extension, one would expect the opposite; the widest fissures should be in the oldest areas. The widest fissures are  $\sim 5$  m. Using simple fracture mechanics, these fissures probably extend all the way through layer 2A and into the sheeted dike sequence. These have been interpreted as eruptive fissures, and this is where high-temperature vents ( $> 300^\circ\text{C}$ ) are concentrated. In contrast to the magma rich, dike-controlled hydrothermal systems that are common on fast-spreading centers, magma-starved hydrothermal systems on slow-spreading ridges tend to be controlled more by the penetration of sea water along faults near the ridge axis. (See **Hydrothermal Vent Deposits**.)

## Faulting

Extension at midocean ridges causes fissuring and normal faulting. The lithosphere is sufficiently thick and strong on slow-spreading centers to support shear failure on the axis, so normal faulting along dipping fault planes can occur on or very close to the axis. These faults produce grabens 1–3 km deep. In contrast, normal faulting along inclined fault planes is not common on fast-spreading centers within  $\pm 2$  km of the axis, probably because the lithosphere is too thin and weak to support normal faulting. Instead, the new thin crust fails by simple tensional cracking.

Fault strikes tend to be perpendicular to the least compressive stress; thus they also tend to be perpendicular to the spreading direction. While there is some ‘noise’ in the fault trends, most of this

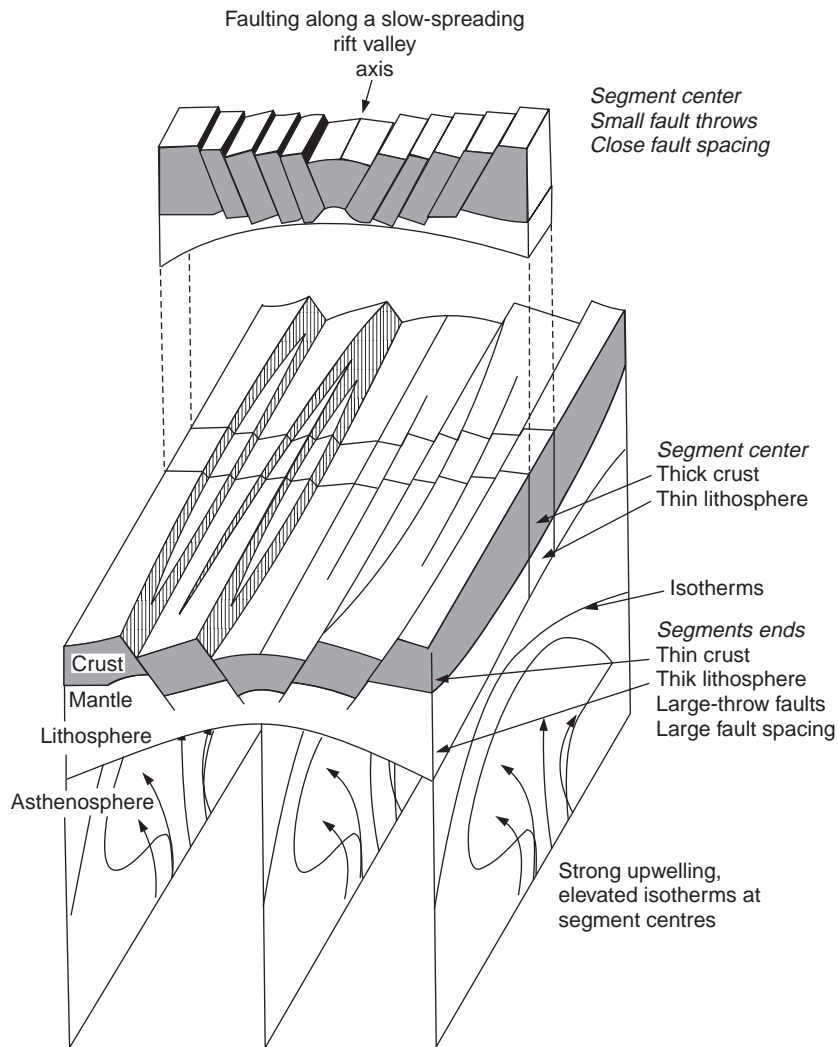


**Figure 11** A geological interpretation for along-axis variations in scarp height, and more closely spaced scarps near mid-segment on a slow-spreading center. Cross-section through segment center (top) shows more closely spaced, smaller-throw faults than at the segment ends (bottom). Focused mantle upwelling near the segment center causes this region to be hotter; the lithosphere will be thinner while increased melt supply creates a thicker crust. In contrast to fast-spreading centers, there may be very little melt redistribution along-strike. Near the segment ends, the lithosphere will be thicker and magma supply is less creating thinner crust. Along axis variations in scarp height and spacing reflect these along axis variations in lithospheric thickness. Amagmatic extension across the larger faults near segments ends may also thin the crust, especially at inside corner highs. Modified from Shaw (1992).

noise can be accounted for by perturbations to the least compressive stress direction due to shearing in the vicinity of active or fossil ridge axis discontinuities. Once this is accounted for, fault trends faithfully record changes in the direction of opening to within  $\pm 3^\circ$  and can be used to study plate motion changes on a finer scale than that provided by seafloor magnetic anomalies. Studies of the cumulative throw of normal faults, seismicity, and fault spacing suggest that most faulting occurs within  $\pm 20\text{--}40\text{ km}$  of the axis independent of spreading rate.

There is a spreading rate dependence for the occurrence of inward and outward dipping faults. Most faults dip toward the axis on slow-spreading centers ( $\sim 80\%$ ), but there is a monotonic increase in the occurrence of outward dipping faults with spreading rate (Figure 10). Inward and outward facing faults are approximately equally abundant at very fast spreading rates. This can be explained by the smaller mean normal stress across a fault plane that dips toward the axis, cutting through thin lithosphere, versus a fault plane that cuts through a much thicker section of litho-

sphere dipping away from the axis. Given reasonable thermal models, the difference in the thickness of the lithosphere cut by planes dipping toward versus away from the axis (and the mean normal stress across those planes) decreases significantly with spreading rate, making outward dipping faults more likely at fast-spreading rates (Figures 10 and 11).

At all spreading rates, important along-strike variations in faulting occur within major (first- and second-order) spreading segments. Fault throws (inferred from scarp heights) decrease in the mid-segment regions away from discontinuities (Figures 8 and 11). This may be caused by a combination of thicker crust, thinner lithosphere, greater magma supply and less amagmatic extension away from RADs in the mid-segment region (Figure 11). Another possible explanation for along-strike variations in fault throw is along-strike variations in the degree of coupling between the mantle and crust. A ductile lower crust will tend to decouple the upper crust from extensional stresses in the mantle, and the existence of a ductile lower crust will depend on spreading rate, the supply of magma to the ridge, and proximity to major discontinuities.

Estimates of crustal strain due to normal faulting vary from 10–20% on the slow-spreading MAR to ~3–5% on the fast-spreading EPR. This difference may be explained as follows. The rate of magma supply to slow-spreading ridges is relatively low compared with the rate of crustal extension and faulting, while extension and magma supply rates are in closer balance on fast-spreading ridges. The resulting seismicity is different too. In contrast to slow-spreading ridges where teleseismically detected earthquakes are common, faulting at fast-spreading ridges rarely produces earthquakes of magnitude > 4. Nearly all of these events are associated with RADs. The level of seismicity measured at fast-spreading ridges accounts for only a very small percentage of the observed strain due to faulting, whereas fault strain at slow ridges is comparable to the observed seismic moment release. It has been suggested that faults in fast-spreading environments accumulate slip largely by stable sliding (aseismically) owing to the warm temperatures and associated thin brittle layer. At slower spreading rates, faults will extend beyond a frictional stability transition into a field where fault slip occurs unstably (seismically) because of a thicker brittle layer.

Disruption of oceanic crust due to faulting may be particularly extreme on slow-spreading ridges near transform faults (Figure 12). Unusually shallow

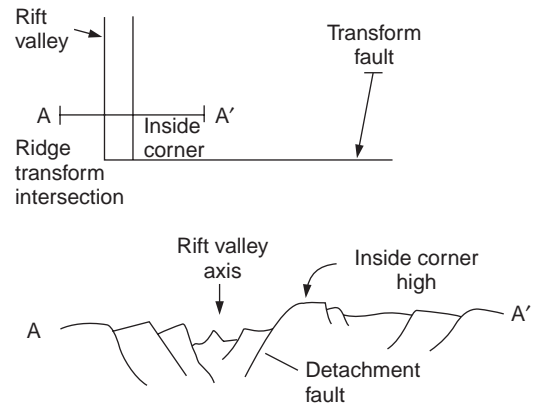


**Figure 12** Inside corner high at a slow-spreading ridge transform intersection. Extension is concentrated along a detachment fault for up to 1–2 million years, exposing deep sections of oceanic crust and mantle. The oceanic crust is thinned by this extreme extension; crustal accretion and magmatic activity may also be diminished.

topography occurs on the active transform slip side of ridge transform intersections; this is called the high inside corner. These highs are not volcanoes. Instead they are caused by normal faults which cut deeply and perhaps all the way through oceanic crust. It is thought that crustal extension may occur for 1 to 2 million years on detachment faults with little magmatic activity. This results in extraordinary extension of the crust and exposure of large sections of the deep crust and upper mantle on the seafloor. Corrugated slip surfaces indicating the direction of fault slip are also evident and are called by some investigators, ‘megamullions.’

At distances of several tens of kilometers off-axis, topography generated near the spreading center is preserved on the seafloor with little subsequent change until it is subducted, except for the gradual accumulation of pelagic sediments at rates of ~0.5–20 cm per thousand years. The preserved topographic highs and lows are called abyssal hills. At slow-spreading centers characterized by an axial rift valley, back-tilted fault blocks and half-grabens may be the dominant origin of abyssal hills (Figure 13), although there is continued controversy over the role of high-angle versus low-angle faults, listric faulting versus planar faulting, and the possible role of punctuated episodes of volcanism versus amagmatic extension. At intermediate-rate spreading centers, abyssal hill structure may vary with the local magmatic budget. Where the budget is starved and the axis is characterized by a rift valley, abyssal hills are generally back-tilted fault blocks. Where the magmatic budget is robust and an axial high is present, the axial lithosphere is episodically thick enough to support a volcanic construction that may

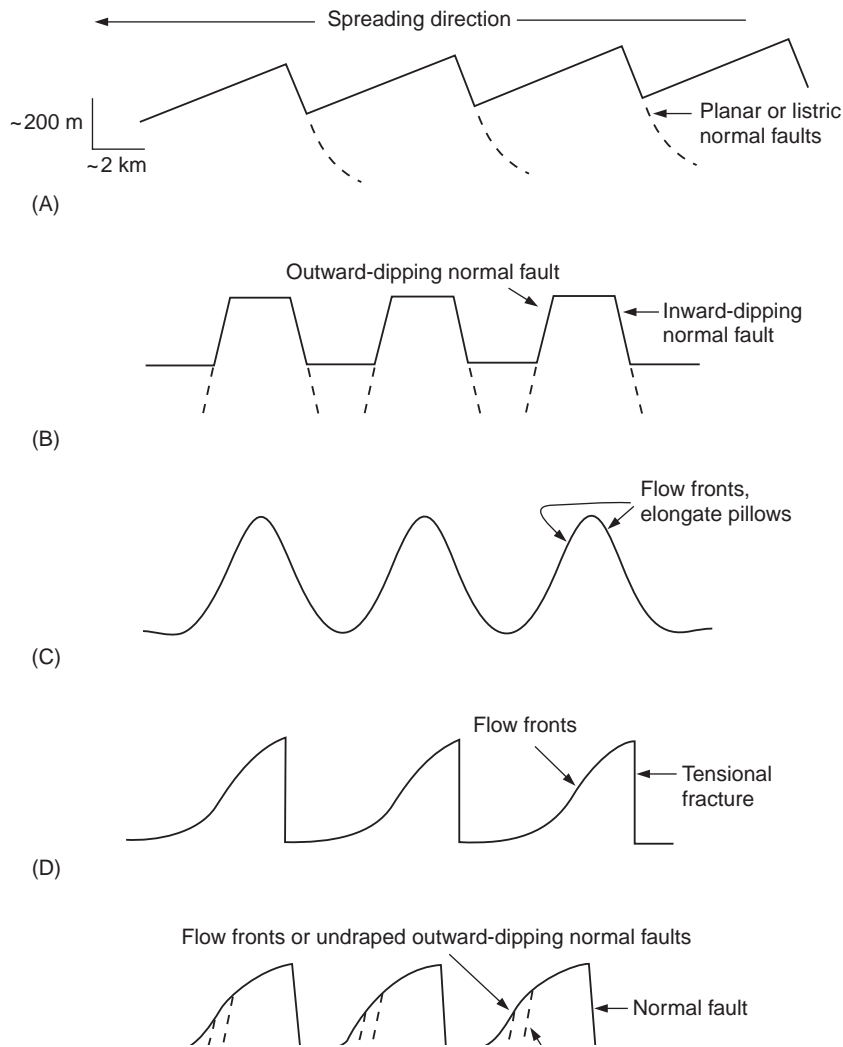


**Figure 13** Five models for the development of abyssal hills on the flanks of midocean ridges. (A) Back-tilted fault blocks (episodic inward-dipping normal faulting off-axis). (B) Horst and graben (episodic inward- and outward-dipping faulting off-axis). (C) Whole volcanoes (episodic volcanism on-axis). (D) Split volcanoes (episodic volcanism and splitting on-axis). (E) Horsts bounded by inward-dipping normal faults and outward-dipping volcanic growth faults (episodic faulting off-axis and episodic volcanism on or near-axis).

then be rafted away intact or split in two along the spreading axis, resulting in whole-volcano or split-volcano abyssal hills, respectively.

Based on observations made from the submersible ALVIN on the flanks of the EPR, the outward facing slopes of the hills are neither simple outward dipping normal faults, as would be predicted by the horst/graben model, nor are they entirely volcanic-constructional, as would be predicted by the split-volcano model. Instead, the outward facing slopes are ‘volcanic growth faults’ (Figure 14). Outward-facing scarps produced by episodes of normal faulting are buried near the axis by syntectonic lava flows originating along the axial high. Repeated episodes of dip-slip faulting and volcanic burial result in structures resembling growth faults, except that the faults are episodically buried by lava flows

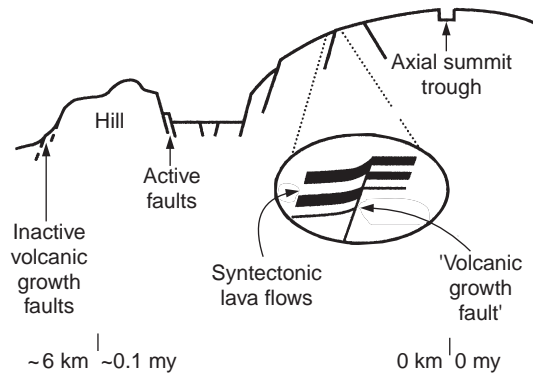


**Figure 14** Volcanic growth faults; cross-sectional depiction of the development of volcanic growth faults. Volcanic growth faults are common on fast-spreading centers and explain some of the differences between inward- and outward-facing scarps as well as the morphology and origin of most abyssal hills near fast-spreading centers.

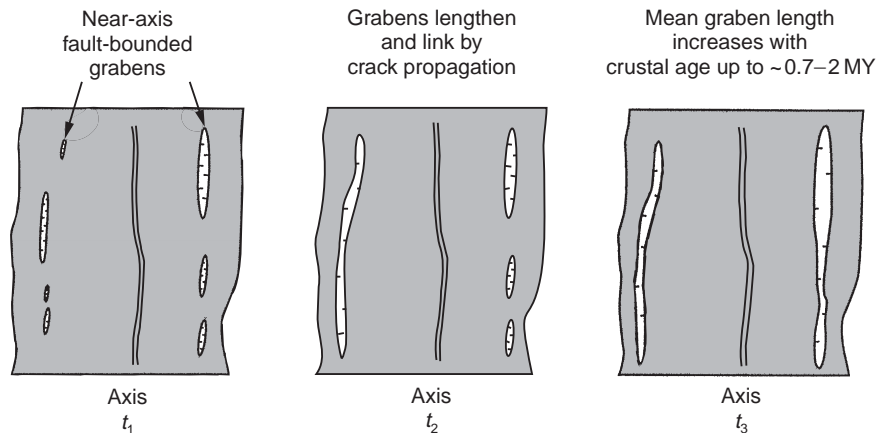


**Figure 15** Proposed time sequence of along-strike propagation and linkage of near-axis faults and grabens that define the edges of abyssal hills; time-averaged propagation rates are approximately 20–60 km per million years.

rather than being continuously buried by sediment deposition. In contrast, the inward dipping faults act as tectonic dams to lava flows. Thus, the abyssal hills are horsts and the intervening troughs are grabens with the important modification to the horst/graben model that the outward facing slopes are created by volcanic growth faulting rather than traditional normal faulting. Thus, on fast-spreading centers, abyssal hills are asymmetric, bounded by steeply dipping normal faults facing the spreading axis, and bounded by a volcanic growth faults on the opposing side (Figure 14). The abyssal hills lengthen at a rate of approximately 60 mm/y for the first  $\sim 0.7$  my by along strike propagation of individual faults as well as by linkage of neighboring faults (Figure 15).

## See also

**Hydrothermal Vent Fluids, Chemistry of. Hydrothermal Vent Deposits. Mid-ocean Ridge Seismic Structure. Mid-ocean Ridge Tectonics, Volcanism and Geomorphology. Propagating Rifts and Microplates.**

## Further Reading

Buck WR, Delaney PT, Karson JA and Lagabrielle Y (1998) *Faulting and Magmatism at Mid-Ocean Rides*. AGU Geophysical Monographs 106. Washington, DC: American Geophysical Union.

Humphris SE, Zierenberg RA, Mullineaux LS and Thompson RE (1995) *Seafloor Hydrothermal Systems: Physical, Chemical, Biological and Geochemical Interactions*. AGU Geophysical Monographs 91. Washington, DC: American Geophysical Union.

Langmuir CH, Bender JF and Batiza R (1986) Petrological and tectonic segmentation of the East Pacific Rise,  $5^{\circ}30'N$ – $14^{\circ}30'N$ . *Nature* 322: 422–429.

Macdonald KC (1982) Mid-ocean ridges: fine scale tectonic, volcanic and hydrothermal processes within the plate boundary zone. *Annual Reviews of Earth and Planetary Science* 10: 155–190.

Macdonald KC and Fox PJ (1990) The mid-ocean ridge. *Scientific American* 262: 72–79.

Macdonald KC, Scheirer DS and Carbotte SM (1991) Mid-ocean ridges: discontinuities, segments and giant cracks. *Science* 253: 986–994.

Menard H (1986) *Ocean of Truth*. Princeton, NJ: Princeton University Press.

Phipps-Morgan J, Blackman DK and Sinton J (1992) *Mantle Flow and Melt Generation at Mid-ocean Ridges* AGU Geophysical Monographs 71. Washington, DC: American Geophysical Union.

Shaw PR (1992) Ridge segmentation, faulting and crustal thickness in the Atlantic Ocean. *Nature* 358: 490–493.

Scheirer DS and Macdonald KC (1993) Variation in cross-sectional area of the axial ridge along the East Pacific Rise: Evidence for the magmatic budget of a fast-spreading center. *Journal of Geophysical Research* 98: 7871–7885.

Sinton JM and Detrick RS (1992) Mid-ocean ridge magma chambers. *Journal of Geophysical Research* 97: 197–216.